Photoionization and electron-impact ionization of the $4d^{10}$ subshell in the palladium isoelectronic sequence

Stephen M. Younger
A-Division, Lawrence Livermore National Laboratory, Livermore, California 94550
(Received 3 April 1986)

Calculations of the electron-impact ionization cross sections and photoionization cross sections for ten ions in the palladium isoelectronic sequence from Ag II to W XXIX were performed using a nonrelativistic single-configuration distorted-wave approximation. The $4d^9kf\,^1P$ partial wave was found to be sensitive to the exchange potential involving $4d$ core electrons, resulting in large qualitative differences between cross sections computed in the term-dependent Hartree-Fock potential and the configuration-averaged potential.

I. INTRODUCTION

In recent years there has been significant progress in understanding radiative and collisional processes occurring in ions that have been ionized a few times.[1] This progress has been the result of both improved computational facilities for the theorist and improved experimental capabilities which allow quantitative measurements of atomic cross sections for multiply charged ions. Most of the calculations and measurements of multiply charged ions have concentrated on few-valence-electron isoelectronic sequences owing to their relative simplicity and their importance for spectroscopic analysis in astrophysical and fusion plasma applications. In the case of photoionization, almost all measurements have been performed on neutral atoms; only a few ions have yet been addressed experimentally.

The study of photoabsorption and electron-scattering processes in heavy, few-times-ionized atoms has several attractions. First, recent calculations[2] and observations[3] of photoabsorption involving electrons of the closed $4d$ subshell in Ba and nearby atoms have revealed dramatic qualitative changes in the photoabsorption spectra due to strong term-dependent exchange potentials occurring in the Hamiltonians describing such states. The study of heavy isoelectronic sequences gives interesting insight to atomic dynamics for cases where orbital exchange effects are quite large and where variation of the charge of the isoelectronic ion allows the relative strength of the interelectronic interaction to be varied with respect to the central nuclear potential. The second reason for studying heavy ions is the increasing availability of experimental facilities which can access multiple ionization states with sufficient populations to allow quantitative cross-section measurements to be performed. Third, the appearance of high-Z elements in advanced inertial confinement fusion capsule designs[4] requires data on the opacities and cross sections of these elements in order for accurate energy-transport calculations to be done.

The present paper reports calculations of the photoionization and electron-ionization cross sections of multiply charged palladiumlike ions which have the ground state $KLM\,4s^24p^64d^{10}\,^1S$. The palladium sequence serves as a prototype for term-dependent effects occurring in other, more complex isoelectronic sequences since it is free of the complicating effects of outer-subshell electrons which could mask the principal term dependence operating between the core and the excited electrons. In a previous paper[5] calculations were reported for the radiative transition probabilities of the resonance transition $4d^{10}\,^1S-4d^94f\,^1P$ in the palladium sequence, revealing dramatic changes in the positions and the shapes of the $4f$ orbitals arising from excited-state term dependence. The present paper extends the study of the palladium sequence by reporting calculations of the photoionization and electron ionization cross sections of Ag II, Cd III, In IV, Sn V, Sb VI, Te VII, Xe IX, Ba XI, Nd XV, and W XXIX.

Section II gives a brief description of the computational method. Section III presents the results and discusses the effect of term dependence on the cross sections. Section IV summarizes the work and suggests other calculations and measurements of interest.

II. COMPUTATIONAL METHOD

The radial orbitals corresponding to the ground-state configuration $KLM\,4s^24p^64d^{10}\,^1S$ were computed in the single-configuration nonrelativistic Hartree-Fock approximation using the computer code of Froese-Fischer.[6] The techniques used for the calculation of the continuum waves employed in the evaluation of the electron-scattering and photoionization matrix elements have been described in several previous publications,[7–9] and only a brief summary will be repeated here. Atomic units will be employed throughout this work. Except where noted energies are given in rydbergs and cross sections in units of πa_0^2, where $a_0=0.529\times10^{-8}$ cm is the Bohr radius.

Previous studies of processes involving transitions of the type nl^{4l+2}-$nl^{4l+1}k(l+1)$ have demonstrated the strong term dependence of the $k(l+1)$ orbital, that is, the strong dependence of the radial structure of the excited orbital on the specific term within the final-state configuration. Indeed, this effect was noted by Hartree and Hartree[10] in an early exchange calculation for the $2s\,2p\,^{1,3}P$

configuration, where the $2p\,{}^1P$ orbital was repelled from the $2s$ by a strong exchange interaction, resulting in a different shaped orbital than that occurring in the $2p\,{}^3P$ configuration which experiences a weaker exchange interaction with the $2s$ electron. The strength of this interaction increases with l, and in heavy ions has been shown to produce an effective double-well potential for the excited electron which can strongly affect the excited orbitals and atomic properties computed from them. Calculations of electron ionization and radiative transitions in argonlike ions,[9] and photoabsorption[3] and electron double ionization[11] out of the $4d$ subshell of several different heavy ions have shown quite dramatically the effects of strong exchange interactions on excited radial orbitals. The d^9 configuration contains ten terms, only one of which, the ${}^1P$, contributes to the photoionization dipole matrix element in LS coupling and to the direct scattering matrix element in the first Born approximation. The radial orbitals corresponding to all but the ${}^1P$ term are close to those resulting from the configuration-averaged wave equation, derived from the Hamiltonian representing the average energy of all of the levels of the configuration. The potential for the kf wave corresponding to the configuration-average (CA) approximation (the potential corresponding to the Hamiltonian for the average energy of the $4d^9kf$ configuration) is[12]

$$V_{\mathrm{CA}}P_{kf}=\left[Z/r-\sum 2Y^0(ns,ns,r)-\sum 6Y^0(np,np,r)-10Y^0(3d,3d,r)-9Y^0(4d,4d,r)\right]P_{kf}$$
$$+\tfrac{1}{7}\sum Y^3(ns,kf,r)P_{ns}+\sum[\tfrac{9}{35}Y^2(np,kf,r)+\tfrac{4}{21}Y^4(np,kf,r)]P_{np}+[\tfrac{3}{7}Y^1(3d,kf,r)+\tfrac{4}{21}Y^3(3d,kf,r)$$
$$+\tfrac{50}{231}Y^5(3d,kf,r)]P_{nd}+\tfrac{9}{10}[\tfrac{3}{7}Y^1(4d,kf,r)+\tfrac{4}{21}Y^3(4d,kf,r)+\tfrac{50}{231}Y^5(4d,kf,r)]P_{4d}\ , \tag{1}$$

where Z is the nuclear charge and where the integral $Y^k(nl,n'l',r)$ is defined as

$$Y^k(nl,n'l',r)=\left[(1/r^{k+1})\int P_{nl}(x)x^kP_{n'l'}(x)dx+r^k\int P_{nl}(x)(1/x^{k+1})P_{n'l'}(x)dx\right]P_{nl}\ . \tag{2}$$

In contrast, the term-dependent Hartree-Fock (TDHF) potential for the $4d^9kf\,{}^1P$ wave is

$$V_{\mathrm{TDHF}}P_{kf}=V_{\mathrm{CA}}P_{kf}+[\tfrac{24}{105}Y^2(4d,4d,r)+\tfrac{66}{693}Y^4(4d,4d,r)]P_{kf}$$
$$-[\tfrac{137}{70}Y^1(4d,kf,r)-\tfrac{2}{105}Y^3(4d,kf,r)-\tfrac{55}{2541}Y^5(4d,kf,r)]P_{4d}\ . \tag{3}$$

It is the large coefficient of the $Y^1(4d,kf,r)$ integral that results in the formation of a strong repulsive potential to occur between the $4d$ subshell and the excited electron, significantly affecting atomic properties involving kf excitations.

Note that not only the f wave experiences term-dependent effects for the d^9kl configuration. Term dependence occurs for all $l\neq 0$ orbitals, although it is relatively weak for the p waves. [For the kp waves appearing in the photoionization calculations we employed the configuration-averaged p-wave potential analogous to Eq. (1).] There is a strong term-dependent component of the d-wave potential for the channel $4d^{10}$–$4d^9kd\,{}^1S$ which appears in the electron-ionization calculations. Except for low incident-electron energies in low charge states, however, the $4d$-kd contribution to the electron-ionization cross section is relatively small, so that even major term-dependent effects will not significantly affect the present results. Also, since the $4d^9kd\,{}^1S$ partial waves are not necessarily orthogonal to the ground-state $4d$ orbital, including term-dependent d waves would require explicit consideration of nonunit overlap integrals in the scattering matrix element, a complication beyond the scope of the relatively straightforward first Born distorted-wave approximation employed here. Orbitals with $l\geq 4$ are much less penetrating at low-to-moderate energies owing to the large centrifugal potential term so that their dependence on the electronic contribution to the potential is weaker than that of the d and f waves.

For the scattering calculation involving electron ionization of a $4d$ electron we are interested in computing Coulomb matrix elements corresponding to the transition:

$$KLM\,4s^24p^64d^{10}k_il_i-KLM\,4s^24p^64d^9k_el_ek_fl_f\ . \tag{4}$$

In this notation the subscripts i, e, and f refer to the incident, ejected, and final (scattered) orbital. Except for the $l=3$ ejected-electron (f-wave) orbitals, all of the continuum waves were computed in central potentials constructed from the Hartree-Fock ground-state radial orbitals corresponding to the initial ion. The potential used for the calculation of the initial and scattered waves was

$$V_{i,f}=[Z/r-\sum Y^0(nl,nl,r)+V_{\mathrm{SCE}}]\ , \tag{5}$$

where V_{SCE} is given by

$$4V_{\mathrm{SCE}}=(V_D-E)+[(V_D-E)^2+a^2]^{1/2} \tag{6}$$

with E the free-electron energy,

$$V_D=V_{i,f}-V_{\mathrm{SCE}}\ , \tag{7}$$

and

$$a=(4/r^2)\sum|P_i(r)|^2\ . \tag{8}$$

V_{SCE} is a local semiclassical exchange (SCE) approximation[13] to the nonlocal exchange potential in Eq. (1) arising from the interaction of the continuum wave with the bound core orbitals. In previous calculations[8] of electron-scattering cross sections this semiclassical exchange potential has been found to accurately reproduce continuum orbitals computed in the configuration-

averaged frozen-core nonlocal Hartree-Fock approximation and offers the advantage of speed of computation for the many hundreds of partial waves involved in a typical ionization cross-section calculation. Thus the initial and scattered continuum waves were computed in an approximation to the configuration averaged potential of the ground state of the initial ion. The ejected waves with $l \neq 3$ were computed in a similar local potential corresponding to the residual ion, i.e., the original ion less the $4d$ electron which has been ionized.

There are several justifications for this choice of scattering potentials. Many studies of the electron-impact ionization of atoms and ions have shown the final cross section to be much less sensitive to the details of the initial and scattered partial-wave potentials than to that of the ejected wave.[7,8] In effect, the scattering orbitals determine a "transition potential" which propagates a one-electron excitation involving the bound and ejected orbitals. The most significant improvements in the distorted-wave description of the electron-impact ionization process are expected to occur in the ejected channel. Furthermore, preliminary studies of the palladium sequence showed a concentration of the cross section in the $l=3$ ejected channels, indicating that the largest improvement in the cross section will occur for improvements in the description of this channel. Note that the SCE approximation to the configuration averaged exchange potential was only employed in the electron impact ionization calculations. For the photoionization studies the nonlocal Hartree-Fock potentials were used.

There are several other approximations inherent in the use of these potentials for photoionization and electron impact ionization calculations. First, they are "frozen-core" potentials in that the continuum wave does not affect the bound orbitals. This approximation is the foundation of the distorted-wave approach to electron scattering and can be removed either by applying the apparatus of a close-coupling approximation or an R-matrix theory, both of which have been developed for single-free-electron calculations.[14] Although such calculations have been applied with success to scattering processes involving one continuum electron, they have not as yet been extended to the case of two free electrons such as occurs in the present study of electron ionization. An intermediate approximation whereby an approximation to the potential term arising from the continuum wave is introduced into the bound-state wave equation is formally more tractable although numerically imposing owing to the many continuum angular momenta and energies occurring in the course of the evaluation of the cross section.

Another approximation used in the present work relates to the interaction of the two continuum waves occurring in the final configuration of the electron-ionization event. The necessity for an approximation arises from the inability of the present simple distorted-wave theory to correctly account for the relative partial-wave phase shift introduced by the interaction of the two final-state continuum orbitals. As a three-body problem, this interaction is not amenable to direct calculation using simple methods, although some significant progress has been made in recent years.[15] In the present work the "maximum interference" exchange approximation of Peterkop[16] is employed. This approximation maximizes the exchange contribution to the cross section and hence minimizes the resulting cross section. In previous calculations of the electron-ionization cross sections of many atoms and ions this approximation has been found to be effective in producing cross sections in good agreement with experimental observations.[17] The very large number of individual transitions corresponding to the many energies and angular momenta of the continuum electrons may average the final-state continuum-continuum interaction to result in reasonably accurate total cross sections.

In order to highlight the systematic variation of the cross section along the isoelectronic sequence we use the reduced energy

$$u = E_i / I \ , \tag{9}$$

where E_i is the energy of the incident photon or electron and I is the ionization energy of the subshell being ionized.

For electron ionization where $u < 2.25$, we used a three-point Gauss-Legendre integration over the final-state energy distribution. Cross sections were summed over partial-wave angular momenta up to 10, 10, and 7, for the initial, scattered, and ejected waves. For $u > 2.25$, a five-point energy integration was employed with maximum partial-wave angular momenta of 14, 14, and 10. These values were found to be adequate to ensure convergence of the cross-section summations to within a few percent at the highest energies and even better at lower energies where the summations are more rapidly convergent. In all cases the cross section was fully converged with respect to the ejected wave, only the initial and scattered waves were found to be slowly convergent. The remaining contribution from higher partial momenta was obtained by extrapolation.

The ionization energies used in the present calculations are given in Table I. For Ag II, Cd III, and In IV experimental values were employed. For the remainder of the ions we use as approximate ionization energies the Hartree-Fock eigenvalues for the orbitals corresponding to the ground state of the initial ion.

III. RESULTS

A. Phase shifts

Figure 1 is a plot of the phase shifts of kf waves computed in the semiclassical exchange (SCE), the (nonlocal) configuration averaged (CA) Hartree-Fock, and the term-

TABLE I. $4d$ subshell ionization energies for palladiumlike ions (Ry).

Ag II 1.580[a]	I VIII 11.27
Cd III 2.754[a]	Xe IX 13.40
In IV 3.96[a]	Ba XI 18.06
Sn V 5.754	Nd XV 29.02
Sb VI 7.446	W XXIX 83.70
Te VIII 9.286	

[a]Experimental.

dependent Hartree-Fock (TDHF) exchange potentials for six ions in the palladium isoelectronic sequence. The good agreement between phase shifts computed in the CA and SCE approximations is remarkable in light of the relative simplicity of the local SCE potential compared to the nonlocal Hartree-Fock expression. At low continuum energy and low ionic charge the bound-state core is compact and the high angular-momentum partial waves are nonpenetrating. The potential experienced by the electron is very nearly Coulombic, resulting in small phase shifts. As the energy is increased, however, there is increased penetration of the continuum electron into the core, resulting in larger phase shifts. Also, as the nuclear charge is increased for fixed free-electron energy the central nuclear component of the potential increases, again causing more core penetration and larger phase shifts. For $Z > 52$ the phase shift is both large at threshold and relatively flat over 0—10 a.u.

In terms of an effective local potential which reproduces the orbitals computed in the actual nonlocal potential one can identify several scenarios. At low ionic charge the direct and exchange contributions to the potential due to the ten $4d$ electrons create a potential barrier in the vicinity of the mean radius of the $4d$ subshell. This barrier divides the overall potential into two wells, the outer of which is very nearly Coulombic. At low continuum energies the free electron does not penetrate the barrier and hence does not have appreciable orbital density in the inner well. Overlap with the bound orbitals is small. As the continuum energy increases there is greater barrier penetration and correspondingly larger phase shifts. When the continuum energy nears the amplitude of the potential barrier there is a dramatic increase in radial orbital density in the inner potential well resulting in rapid energy-dependent changes in the physical properties computed from them. A similar effect occurs at fixed free-electron energy as the nuclear charge is increased. Since the $4d$ orbital changes relatively slowly with Z, so does its contribution to the continuum wave potentials. The net effect of increasing Z is then to shift the barrier downward in energy, reducing the continuum energy required to obtain appreciable radial orbital density in the inner well. Thus as the nuclear charge increases one expects a more rapid increase in phase shift with electron energy. At very high Z, the nuclear potential dominates subshell contributions so that large phase shifts occur even at threshold.

For low ionic charge and low ejected-electron energy the phase shifts for kf waves computed in the TDHF approximation differ significantly from those computed in the CA and SCE potentials. As was noted above, the TDHF wave equation for the $kf\,{}^1P$ wave is strongly affected by the $Y^1(4d,rf,r)$ repulsive potential term. This term is a major component in the strengthening of the effective potential barrier which prevents core penetration by the high-angular-momentum kf wave. A much higher nuclear charge or continuum wave energy is required to overcome the barrier in the TDHF approximation com-

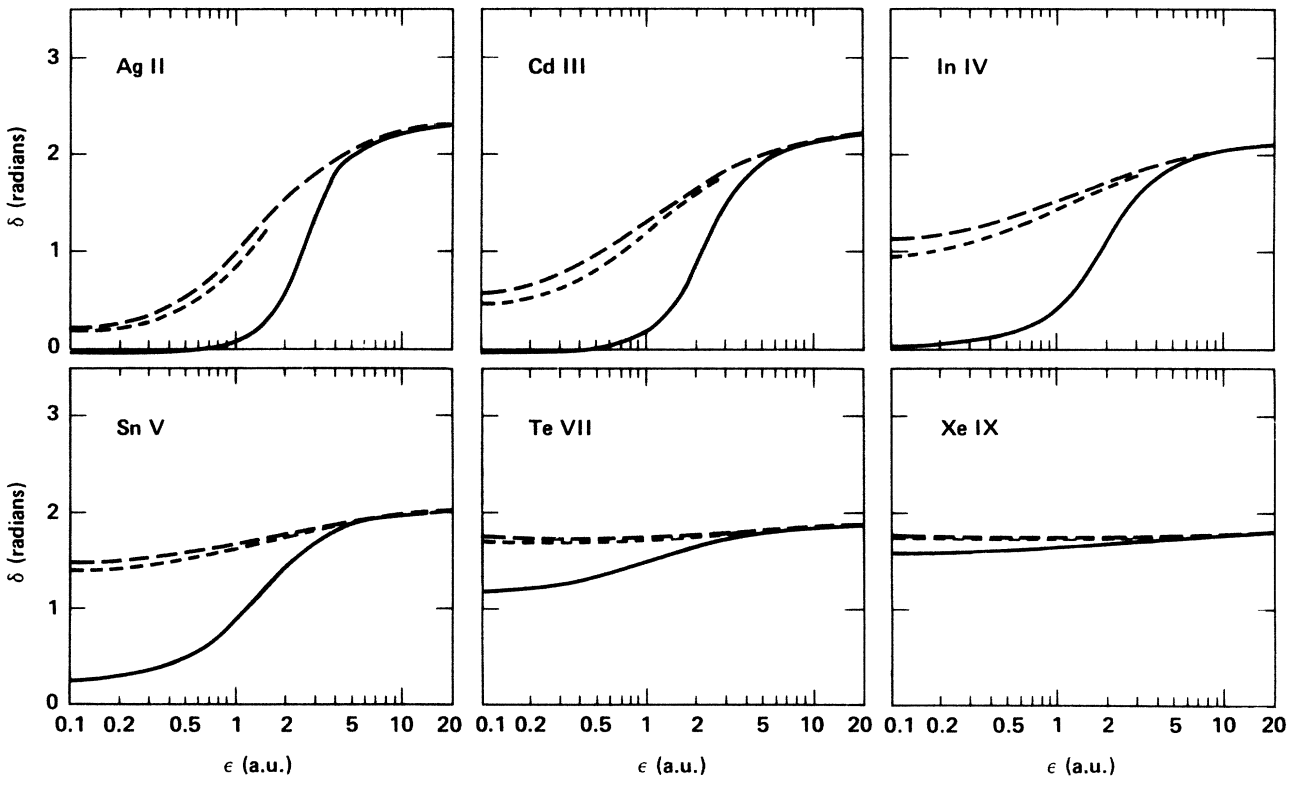

FIG. 1. Partial-wave phase shifts for $l = 3$ orbitals in the TDHF (solid line), the CA (long-dashed line), and the SCE (short-dashed line) potential approximations. ϵ is the ejected energy in a.u.

pared to the CA approximation. The $kf\,^1P$ wave phase shifts for the TDHF approximation clearly illustrate this effect. For Ag II the threshold TDHF phase shift is small and increases slowly with energy. For Cd III the increase in phase shift with increasing energy is much more rapid than in Ag II indicative of increasing core penetration. For In IV and Sn V the threshold phase shift is again small, but increases rapidly with energy, corresponding to a weakening effect of the potential barrier. At higher charge states the threshold phase shift increases, approaching the CA values. In all cases the TDHF phase shift increases more slowly with increasing electron energy than those computed in the CA potential. Note also that the TDHF and SCE phase shifts begin to converge at lower relative energies as the nuclear charge increases, reflecting the relative lowering of the potential barrier by the increasing nuclear potential.

B. Photoionization cross sections

Photoionization cross sections for the ions Ag II, Cd III, In IV, Sn V, Sb VI, Te VIII, I VIII, Xe IX, Ba XI, and Nd XV, computed in the configuration-averaged and term-dependent exchange approximations are shown in Fig. 2. The variation with Z of the energy dependence of the photoionization cross section is closely correlated with that of the f-wave phase shift. For Ag II, the cross section is finite at threshold and increases rapidly to a delayed maximum as the f wave penetrates the potential barrier. It then decreases to a Cooper minimum at a free-electron energy of approximately 9 Ry. For Cd III the cross section peaks at a lower free electron energy than in silver, although the peak value is similar. As the nuclear charge is increased and the amplitude of the potential barrier separating the inner and outer potential wells decreases the maximum in the photoionization cross section and the position of the Cooper minimum move to lower free-electron energies. It is interesting to note that in the TDHF approximation Sn V has the largest peak photoionization cross section of any ion in the palladium isoelectronic sequence. As one would expect from the discussion of the last section there are qualitative differences in photoionization cross sections computed with CA and TDHF partial waves owing to the much stronger potential barrier occurring in the later for low charge states. The more rapid shift of radial continuum orbital density into the inner well which occurs for the CA orbitals causes the delayed maximum in the cross section to shift to lower energies than in the TDHF case. Only for $Z > 50$ do the cross sections computed from CA and TDHF partial waves coalesce as the nuclear charge dominates the interelectronic contribution to the partial-wave potentials.

The difference in the energy dependence of the CA and TDHF cross sections thus reflects the differences in the potentials in which the corresponding partial waves were computed. Note, however, that the shape of the photoionization cross-section curves is really a reflection of the degree of overlap between the $4d$ and kf orbitals occurring within the dipole matrix element. Since the $4d$ orbital has two nodes there is the possibility of cancellation occurring in the dipole matrix element radial integral, and it is this cancellation that leads to the zeros in the cross section at various energies, the so-called Cooper minima. Cognizant of these effects, it is apparent that there is a dramatic rearrangement of the photoionization cross section of palladiumlike ions due to the strong term dependence in the ejected wave potential.

It is of interest to compare the Z dependence of the photoionization cross sections of Fig. 2 with that of the oscillator strengths for the $4d^{10}$–$4d^9 4f\,^1P$ transition computed in similar exchange potential approximations.[5] For this resonance transition the f value is small for Ag II because the $4f$ orbital is in the outer potential well and has only a small overlap with the $4d$ orbital. As the nuclear charge increases the $4f$ orbital is pulled closer to the nu-

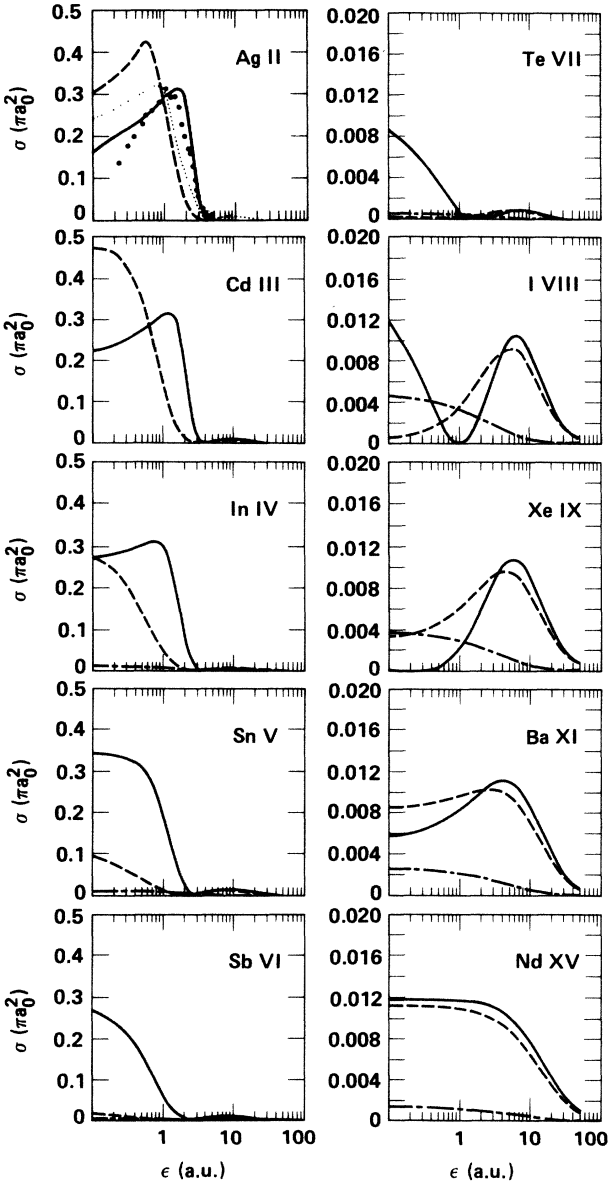

FIG. 2. Photoionization cross sections for palladiumlike ions corresponding to partial waves computed in the TDHF (solid line) and the CA (long-dashed line) potential approximations for $l=3$ orbitals. Also shown is the $4d$-kp cross section (——·——) which was computed using the CA approximation $l=1$ partial waves. ·····, Cooper, Ref. 19. ●, Krause *et al*, Ref. 18. ϵ is the ejected energy in a.u.

cleus and the $4d$ subshell, causing increased overlap with the $4d$ orbital and rapidly increasing oscillator strengths. This increase is much more rapid for $4f$ orbitals computed in the configuration average approximation than in the TDHF approximation, owing to the much larger repulsive exchange term present in the later approximation. The $4f$ orbital is fully contracted at Sn ($Z=50$) in the configuration averaged approximation, whereas in the TDHF approximation collapse is delayed until Ce ($Z=58$). The $4d$-$4f$ oscillator strength reflects these differences. Oscillator strengths computed in the CA approximation rise much more rapidly with Z and peak at lower Z than those which use $4f$ orbitals computed in the TDHF approximation.

Since the total oscillator strength arising from the $4d^{10}$ subshell must be conserved, there is a direct correspondence between the strengths of the bound-bound and the bound-free transitions. For Ag II the bound-bound oscillator strength is small. In order to satisfy the sum rules, this implies that the bound-free component is large, as is the case in Fig. 2. As the nuclear charge increases the $4d$-$4f$ oscillator strength increases, leading to a decrease in the integrated oscillator strength in the continuum. To the extent that different orbital potentials result in different nf mean radii and kf continuum phase shifts there will be corresponding differences in excitation and ionization cross sections. In Te VII the effect is especially pronounced. For this ion the $4f$ CA function is fully collapsed, with a large bound-bound oscillator strength and a corresponding small photoionization cross section. In the TDHF approximation for the same ion, however, the $4f$ orbital is only partially collapsed into the $4d$ subshell, with a smaller bound-bound oscillator strength and a larger photoionization cross section. Te VII is a particularly clear demonstration of the oscillator strength sum rules demonstrating that what is gained in the bound-bound transitions is lost in the continuum, and vice-versa.

Another illustration of the systematic variation of the photoionization cross section along the isoelectronic sequence and the transfer of oscillator strength from the continuum to the bound excitations is shown in Fig. 3, where the TDHF cross sections are plotted vs incident photon energy. All of the cross-section curves share a similar shape, with the ionization threshold, the location of the Cooper minimum, and the second cross-section maximum moving to higher photon energy with increasing nuclear charge. The collapse of the nf orbitals with the concurrent increase in bound-bound oscillator strengths is apparent from the rapid decease in the first maximum of the photoionization cross section between In IV and I VIII.

The $4d$-kp contribution to the photoionization cross

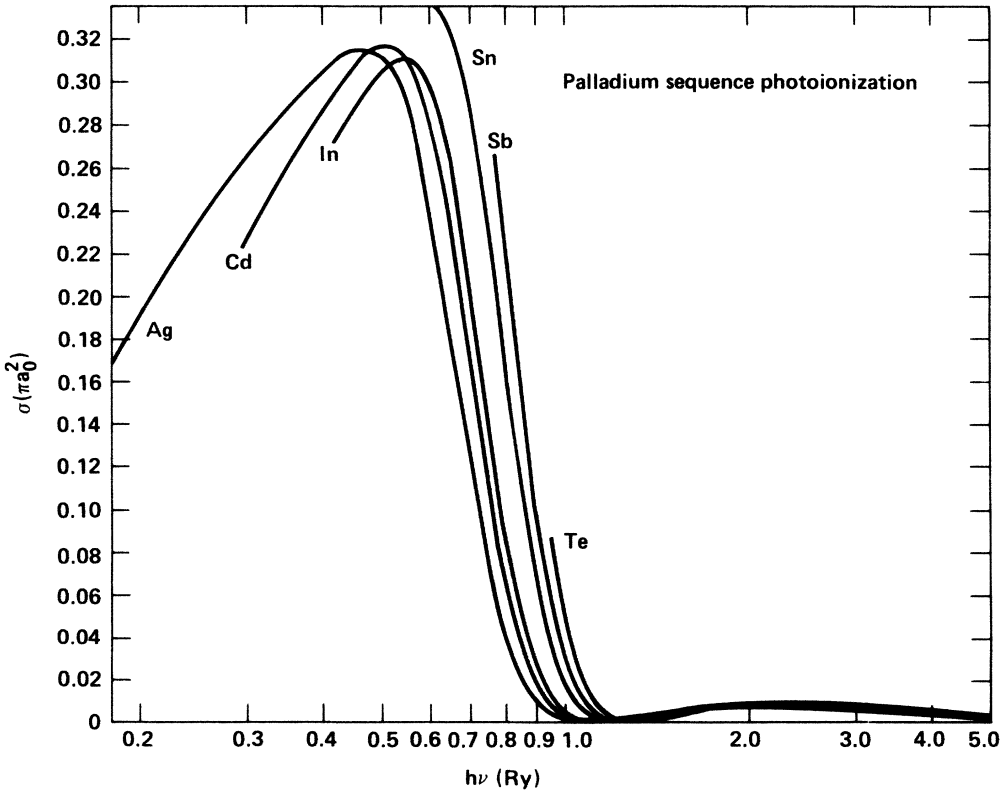

FIG. 3. Plot of the photoionization cross sections of the first six ions of the palladium isoelectronic sequence vs the incident photon energy.

section computed with CA p-waves is much smaller than the f-wave contribution except in the intermediate Z range where the $l=3$ channel undergoes a Cooper minimum near or slightly below threshold. As a check, TDHF p-wave calculations were performed for CD III and Sb VI with the resulting cross sections differing by less than 20% from the CA values.

Experimental data on the photoionization cross sections of palladiumlike ions are not yet available. The present data for singly ionized silver, however, are in reasonable agreement with the measurements of Krause *et al.*[18] for neutral silver over the energy range where ionization from the $4d$ subshell dominates the cross sections (see Fig. 2). Since Krause *et al.* performed relative measurements, for the purposes of comparison we have normalized their values to our own peak TDHF cross section of $0.315\pi a_0^2$. Also shown in this figure are the theoretical results of Cooper[19] for Ag II computed with a central field potential constructed from Hartree-Fock orbitals. Cooper's cross sections are in reasonable agreement with the present results computed in the configuration-averaged approximation. Finally, some recent unpublished calculations of Cheng[20] using the relativistic random-phase approximation are quite similar to the TDHF cross sections.

C. Electron-impact ionization cross sections

Distorted-wave electron-impact ionization cross sections for ten ions of the palladium isoelectronic sequence over the incident electron energy range from threshold to five times the ionization energy are given in Table II. Two values are given for each energy for the ions Ag II to Ba XI, one corresponding to cross sections computed using partial waves generated in the SCE potential (cross sections in parentheses) and the other value corresponding to cross sections derived from TDHF f waves. (Recall that SCE partial waves were employed in all cases for $l\neq 3$ partial waves.) For comparison purposes we also list in Table II scaled cross sections derived from the scaled hydrogenic approximation of Golden and Sampson[21] and Lotz.[22] The scaled hydrogenic approximation computes cross sections using hydrogenic orbitals and relies on scaling laws to relate the results to specific ions of interest. It has proven effective in describing electron ionization for ions where the nuclear charge exceeds the number of electrons by more than a factor of 2. The Lotz formula

$$uI^2Q = 2.77N_{nl}\ln(u)\ , \tag{10a}$$

where uI^2Q is expressed in units of $\pi a_0^2\mathrm{Ry}^2$ and N_{nl} is the

TABLE II. Scaled electron-impact ionization cross sections uI^2Q for palladiumlike ions (units of πa_0^2 Ry^2).

Ion	$u=1.25$	$u=1.5$	$u=2.25$	$u=3.5$	$u=5.0$
Ag II	1.13	2.49	8.96	24.9	38.3
	(2.18)[a]	(4.74)	(16.3)	(39.1)	(53.3)
Cd III	6.00	11.2	26.9	45.5	61.9
	(8.04)	(17.5)	(43.5)	(57.7)	(68.1)
In IV	9.54	18.5	38.7	58.0	74.9
	(15.6)	(27.8)	(40.7)	(49.4)	(60.6)
Sn V	15.9	27.6	46.1	65.3	80.9
	(15.4)	(21.8)	(28.6)	(38.6)	(47.2)
Sb VI	16.7	25.0	39.0	54.9	67.6
	(10.0)	(14.4)	(22.3)	(31.9)	(39.3)
Te VII	10.5	16.1	27.6	39.5	48.5
	(7.12)	(11.4)	(20.3)	(30.1)	(37.6)
Xe IX	5.80	10.3	20.5	31.8	40.7
	(5.96)	(10.6)	(20.7)	(31.4)	(39.7)
Ba XI	6.38	11.4	22.3	33.9	43.1
	(6.34)	(11.4)	(22.3)	(33.7)	(42.3)
Nd XV	(7.37)	(13.0)	(24.5)	(36.3)	(45.0)
W XXIX	(8.69)	(14.8)	(26.6)	(37.2)	(44.4)
Z Expansion (Ref. 21)	9.80	16.1	27.2	36.5	42.4
Lotz (Ref. 22)	6.18	11.2	22.5	34.7	44.6

[a]Cross sections computed using the SCE potential are given in parentheses.

number of electrons in the subshell to being ionized, has proven a simple and surprisingly accurate representation of electron ionization for a wide class of multiply charged ions and is widely used in the absence of more accurate data.

In order to allow easier interpretation and extrapolation of the present calculations to other energies and ions of interest we have fit the scaled TDHF cross sections, ul^2Q, to the expression

$$ul^2Q = A(1-1/u)+B(1-1/u)^2 + C\ln(u)+D\ln(u)/u \ . \quad (10b)$$

A, B, and D are free parameters determined by a least-squares fit to the computed cross sections.[23] C is the Bethe coefficient which determines the slope of the cross section at high incident electron energies and is related to the photoionization cross section

$$C=(I/\pi\alpha)\int[Q/(I+E)]dE \ , \quad (11)$$

where I is the ionization energy in rydbergs, Q is the TDHF photoionization cross section in $\pi\alpha_0^2$, α is the fine-structure constant, and E is the free electron energy. In this representation the computed cross sections completely determine the fit at low incident electron energies and also govern the amplitude of the high-energy component. The slope of the high-energy tail of the cross section is determined by the Bethe coefficient. In previous calculations[23] of electron impact ionization cross sections this expression has proven an accurate expression for the cross section over an extended energy range. In the present work, the smooth distribution of the cross section over ejected partial-wave angular momenta, often with nondipole channels contributing most of the total. In argon[9] and in the $4d$ inner-shell ionization of xenon ions,[11] other cases where term-dependent partial wave effects are important, dipole excitations are quite strong. In such cases satisfactory agreement between theory and experiment is obtained only when term-dependent partial waves are employed. The effects of term dependence are expected to be much larger in the palladium sequence than in the argon sequence owing to the greater relative importance of exchange arising from the ten-electron $4d$ core compared to the six-electron $3p$ core in argonlike ions.

In Table II one notes that the effect of employing term-dependent $l=3$ ejected waves for the lower ionization stages is to delay the maximum in the cross section

TABLE III. Fitting coefficients for Eq. (10).

Ion	A	B	C	D
Ag II	110	−93.0	34.6	−140
Cd III	−12.2	−0.606	47.4	−13.2
In IV	−93.7	56.8	54.6	78.9
Sn V	8.62	−40.8	58.5	18.5
Sb VI	173	−148	38.6	−117
Te VII	161	−89.3	8.46	−114
Xe IX	95.0	−37.1	7.89	−75.5
Ba XI	84.6	−31.6	10.2	−64.4
Nd XV	61.4	−17.5	12.2	−38.9
W XXIX	42.4	−5.46	11.0	−11.6

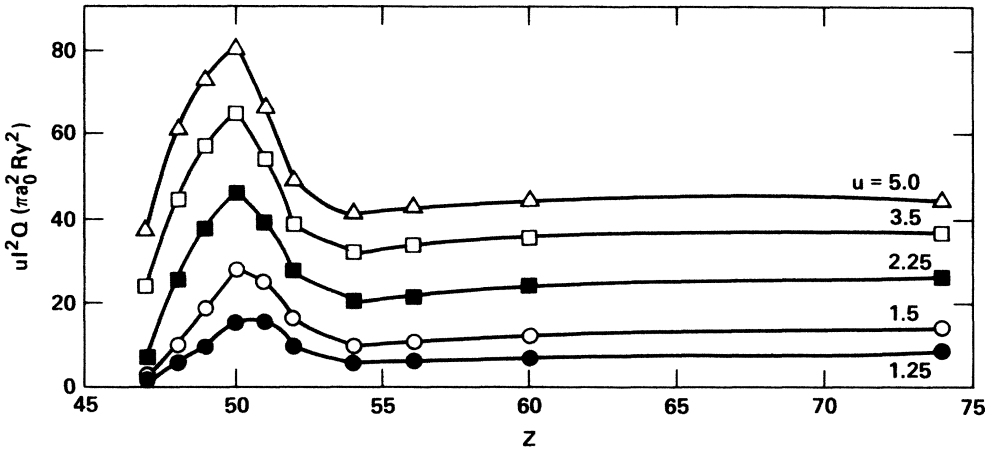

FIG. 5. Isoelectronic plot of the scaled TDHF electron-impact ionization cross sections for palladiumlike ions vs Z.

occurring in electron ionization have a more complex form than the simple one-electron radial integral which determines the photoionization cross section. The two-electron Coulomb matrix element does not lend itself to the formation of the scattering analogy of Cooper minima. To the extent that other ejected partial waves are important in determining the total cross section the effects of $l=3$ term dependence will be masked. Although the partial electron ionization cross section versus ejected electron energy does peak at low energy, where the effects of term dependence are largest, it does include a higher-energy component which is less susceptible to term-dependent effects. Figure 4 plots the scaled cross section I^2Q for Ag II, Cd III, Sb VI, and W XXIX, showing significant variations in the shape of the curves as the nuclear charge is increased.

As was discussed above for photoionization, such term-dependent partial wave effects are expected to disappear at high Z as the nuclear component of the potential dominates the details of the interelectronic interaction. In order to illustrate the systematic variation of the electron-ionization cross section along the isoelectronic sequence we plot in Fig. 5 the scaled cross section ul^2Q versus Z for five incident-electron energies. The maximum scaled cross section occurs at Sn V. It is interesting that in this heavy isoelectronic sequence significant exchange interactions persist until the tenth ionization stage. In lighter sequences such effects usually disappear within the first few ionization stages.[8,9] In Table II one notes that in the intermediate-Z range the SCE and TDHF electron ionization cross sections differ by more than a factor of 2.

There is currently no experimental data available for the electron ionization of ions in the palladium sequence. This is unfortunate since the Pd sequence represents a particularly clean test of the ability of partial-wave theories to describe electron ionization from heavy ions where direct ionization is expected to be the dominant contribution to the total electron-ionization cross section. Complications in the interpretation of the direct cross section owing to the appearance of strong excitation-autoionization resonances are expected to be much weaker in the Pd sequence than in other heavy ions, allowing a comparison of direct-ionization theory and experiment. Measurement of several ions along the sequence would provide a demonstration of the systematic variation of the strength of the exchange interaction in a region where partial-wave potential effects are expected to produce factor of 2 changes in the total single-ionization cross section.

IV. SUMMARY

We have presented distorted-wave calculations of the photoionization and electron-ionization cross sections for ten elements of the palladium isoelectronic sequence. Particular attention was given the importance of the $l=3$ ejected electron potential in determining the cross section. Large deviations between results computed in configuration-averaged and term-dependent $l=3$ partial wave potentials were found up to the tenth charge state, illustrating the persistant strength of the $4d$-kf exchange interaction along the isoelectronic sequence.

The current calculations do not include consideration of electron correlation beyond the level of the Hartree-Fock approximation used to compute the bound state and continuum orbitals. Previous calculations of the photoionization of Ba^{2+} and the electron ionization of neutral argon, both of which have similar $nl^{4l+2}-nl^{4l+1}k(l+1)$ excitations, both resulted in reductions of the peak cross sections on the order of 20—30%, much less than the factor of 2 reductions caused by the use of term-dependent partial waves. Intermediate coupling effects might also be significant at the higher charge states. Both of these additional channel interactions would serve as vehicles for the further redistribution of oscillator strength beyond the single channel interaction (term dependence) considered here. Even within the single configuration LS coupling representation, however, it is apparent that the direct electron ionization of heavy few-times-ionized atoms is con-

siderably more complex than is the case for lighter ions which have received the greatest attention in recent years. Experimental observation of such systems would provide a more strict test of the distorted wave approach to electron scattering than has heretofore been possible.

ACKNOWLEDGMENTS

This work was performed under the auspices of the U. S. Department of Energy by Lawrence Livermore National Laboratory under contract No. W-7405-Eng-48.

[1]R. D. Cowan., *The Theory of Atomic Structure and Spectra* (University of California Press, Berkeley, 1981).
[2]K. T. Cheng and W. R. Johnson, Phys. Rev. A **28**, 2820 (1983).
[3]T. B. Lucatorto, T. J. McIlrath, J. Sugar, and S. M. Younger, Phys. Rev. Lett. **16**, 1124 (1981).
[4]J. D. Lindl and J. W. -K. Mark, Lasers Part. Beams **3**, 37 (1985).
[5]S. M. Younger, Phys. Rev. A **22**, 2682 (1980).
[6]C. Froese-Fischer, Comput. Phys. Commun. **14**, 145 (1978).
[7]S. M. Younger, Phys. Rev. A **22**, 111 (1980).
[8]S. M. Younger, Phys. Rev. A **23**, 1138 (1981).
[9]S. M. Younger, Phys. Rev. A **26**, 3177 (1982).
[10]D. H. Hartree and W. Hartree, Proc. R. Soc. London, Ser. A **154**, 588 (1936).
[11]M. S. Pindzola, D. C. Griffin, C. Bottcher, D. H. Crandall, R. A. Phaneuf, and D. C. Gregory, Phys. Rev. A **29**, 1749 (1984).
[12]E. U. Condon and H. Odabasi, *Atomic Structure* (Cambridge University Press, Cambridge, 1980).
[13]M. E. Riley and D. G. Truhlar, J. Chem. Phys. **63**, 2182 (1975).
[14]R. J. W. Henry, Phys. Rep. **68**, 1 (1981).
[15]F. H. Read, in *Electron Impact Ionization,* edited by T. D. Mark and G. H. Dunn (Springer-Verlag, Vienna, 1985), Chap. 3.
[16]R. K. Peterkop, Zh. Eksp. Teor. Fiz. **41**, 1938 (1961) [Sov. Phys.—JETP **14**, 1377 (1962)].
[17]S. M. Younger, in *Electron Impact Ionization,* edited by T. D. Mark and G. H. Dunn (Springer-Verlag, Vienna, 1985), Chap. 1.
[18]M. O. Krause, W. A. Svensson, T. A. Carlson, G. Leroi, D. E. Ederer, D. M. P. Holland, and A. C. Parr, J. Phys. B **18**, 4069 (1985).
[19]J. W. Cooper, Phys. Rev. **128**, 681 (1962).
[20]K. T. Cheng (private communication).
[21]L. B. Golden and D. H. Sampson, J. Phys. B **13**, 2645 (1980).
[22]W. Lotz, Z. Phys. **216**, 241 (1968).
[23]S. M. Younger, J. Quant. Spectrosc. Radiat. Transfer **25**, 329 (1981).